Draft: Advanced Material Interfaces, 2021, *8 (14)*, 2100370.

Electrostatics of Single Monolayer Graphene Coated Metal Electrode in Electrolyte

Akshat R. Saraf[1], Kamran Keramatnejad[2], Jennifer A. Arcila[3], Ravi F. Saraf[3,*]

[1]Department of Nanoengineering, University of California at San Diego, La Jolla, CA 92093; [2]Vajra Instrument, Lincoln, NE 58512; [3]Department of Chemical and Biomolecular Engineering, University of Nebraska – Lincoln, NE 68588.

The Table of Contents (TOC) and Figure abstract

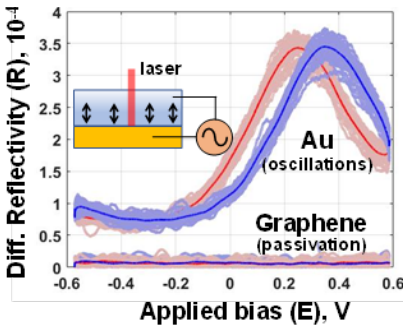

The oscillation of ions due to applied AC potential is completely passivated due to a monolayer of graphene in an electrolyte. The passivation is observed as differential reflectivity as a function of applied DC potential E from -0.6 to 0.6 V.

Electrostatics of Single Monolayer Graphene Coated Metal Electrode in Electrolyte

Akshat R. Saraf[1], Kamran Keramatnejad[2], Jennifer A. Arcila[3], Ravi F. Saraf[3,*]

[1]Department of Nanoengineering, University of California at San Diego, La Jolla, CA 92093; [2]Vajra Instrument, Lincoln, NE 58512; [3]Department of Chemical and Biomolecular Engineering, University of Nebraska – Lincoln, NE 68588.

ABSTRACT

Unlike metals, graphene forms a hydration layer at the electrode/electrolyte interface, which is unusual for a conducting material. Here, the electrostatic properties of the hydration layer were studied by measuring the oscillation of ions at the interface due to an applied AC potential by differential reflectivity during cyclic voltammetry (CV). The amplitude of ion oscillation at picometer range sensitivity on a partially coated Au electrode by a graphene monolayer reveals a remarkable difference between the coated and uncoated part of the electrode. The uncoated Au electrode exhibits the expected behavior, but the oscillation of ions was completely screened over the graphene coated electrode up to 200 mM of NaCl. The "insulating" behavior was consistent with CV and DPV. The behavior attributed to the hydration layer could be reversibly disrupted to de-screen the electric field to study the electrostatics of graphene/Au interface. The shift in Fermi level of hydration-layer-free graphene/Au relative to Au is quantitatively consistent with work function transparency of graphene. The cut-off of the emanating field from the underlying electrode in an electrolyte is another example of graphene's unique passivation property that will have profound effect on applications such as, supercapacitors where the charge state of interface is critical.

Keywords: electrical double layer; hydration layer; graphene electrochemistry; Helmholtz layer; hydrophobic interfaces, differential reflectivity, potential of zero charge

The electrostatics of graphene/electrolyte interface is central to developing their applications such as, supercapacitors for energy devices[1] and electrochemical field effect transistors (eFETs) for chemical sensing.[2] The complexity of graphene interfaces with electrolytes emerge from two rather disparate properties. Like oxide-free noble metals, graphene is electrically conducting.[3] However, similar to other carbonaceous materials, it is considered largely hydrophobic,[4] given some contribution form hydrocarbon contamination on the surface.[5] As a result, the ions will be attracted to the surface due to conductivity (i.e., image charge), but the hydrophobicity will tend to repel them.[6] As a result, the interface of electrolyte with graphene is unusual. It is experimentally shown by x-ray reflectivity[7] and supported by simulation[7] that the interface of graphene supported on a metal will also have an ~1 nm thick low density water layer (also called "vacuum layer"), consistent with other hydrophobic surfaces.[8] To reconcile the hydrophobic and electrically conducting nature of graphene, simulation studies show a formation of a "hydrophobic" hydration layer on the interface between the graphene and the bulk aqueous solution;[4a, 9] There are two hydration layers, at ~0.3 and ~0.6 nm, and the ions in the solution

appear to disrupt the layer farther from the interface.[9b] Simulation of electrowetting on graphene/metal surface show that the polarization of hydration layer causes dramatic and complete screening of the electric field on graphene.[9c] It was estimated, that hydration screens over 85% of ion-graphene molecular electric field.[9d] Simulation on the dynamics of the hydration layers show that the negative potential is more disruptive.[9e] Experimentally, the formation and the structure of hydration layer was measured by scanning probe microscopy[10] and x-ray reflectivity.[11] An interesting experimental evidence of the hydrophobic hydration layer is the reversible wettability of graphene on UV exposure that form oxygen and hydroxyl radicals that react with graphene to make the interface hydrophilic which can be reversed to hydrophobic surface on storing in the dark.[12] By contrast, simulations of density fluctuations at the interface point to a hydrophilic nature of graphene,[13] which have also been concluded by contact angle measurements on free standing films.[14] Furthermore, the low density of states compared to metals at the Dirac Point gives rise to quantum capacitance that lowers the overall interfacial capacitance.[15] Thus, the electrostatics of electrolyte/graphene interface that affects a range of electrochemical application remains a subject of intense research with potentially undiscovered phenomenon.

Here, the dynamic nature of the interface was experimentally studied by differential reflectivity to probe the electrostatics of the interface, particularly the dielectrics and mechanical stability of the hydration layer. Due to the atomic thickness of graphene, the underlying substrate strongly affects the wetting properties;[16] and the intrinsic electronic properties, such as work function and Fermi level.[17] The study is confined to electrolyte/graphene/Au (substrate) structure. The primary result is a surprising finding: Unlike a metal electrode, the coating of a single layer of graphene efficiently screens the electric field emanating from the underlying Au electrode. The high screening is attributed to the formation of a charge-free, dielectric hydration layer shown by simulation.[4, 9] The hydration layer can be reversibly disrupted by AC potential; however, its healing appears to be a slow process, perhaps attributed to the requirement of obtaining a topologically precise hydrogen bonding with no dangling bonds to make the layer hydrophobic. The estimated magnitude of effective potential of zero charge (PZC) of hydration stripped graphene shows a higher Fermi level than pristine Au that is consistent with the electronic transparency of graphene monolayer reported in the literature. Although there have been simulation studies,[4a, 9] to our knowledge this is the first direct experimental evidence that shows the (complete) electric field screening due to hydration layer polarization; furthermore, by reversibly disrupting the hydration layer the quantitative transparency of the graphene is shown as a shift the Fermi level (i.e., PZC) relative to the aqueous media.

RESULTS AND DISCUSSION

The samples were graphene monolayer crystals on Au electrode supported on Si chip (Figure 1(a)). Details of the sample preparation to deposit the Au electrode on a Si chip are given in the Method Section. Raman spectrum was measured on several spots on the chip before and after the removal of the polymer backing. Before the removal of the polymer film, four additional peaks were observed (Figure 1(b)). After dissolving the polymer, the classic Raman spectrum of

graphene with 2D and G peaks[18] was observed, where the ratio of former being nominally twice that of latter indicating high quality of the graphene monolayer. Well over ten spots over each chip was measured to ensure robustness of the process and map the approximate location of the graphene flakes (Figure S1, Supporting Information (SI)). The chip had numerical markers patterned during lithography to map the location of the graphene a priori (Figure S2, SI) using the Raman imaging microscope (Figure S1, SI).

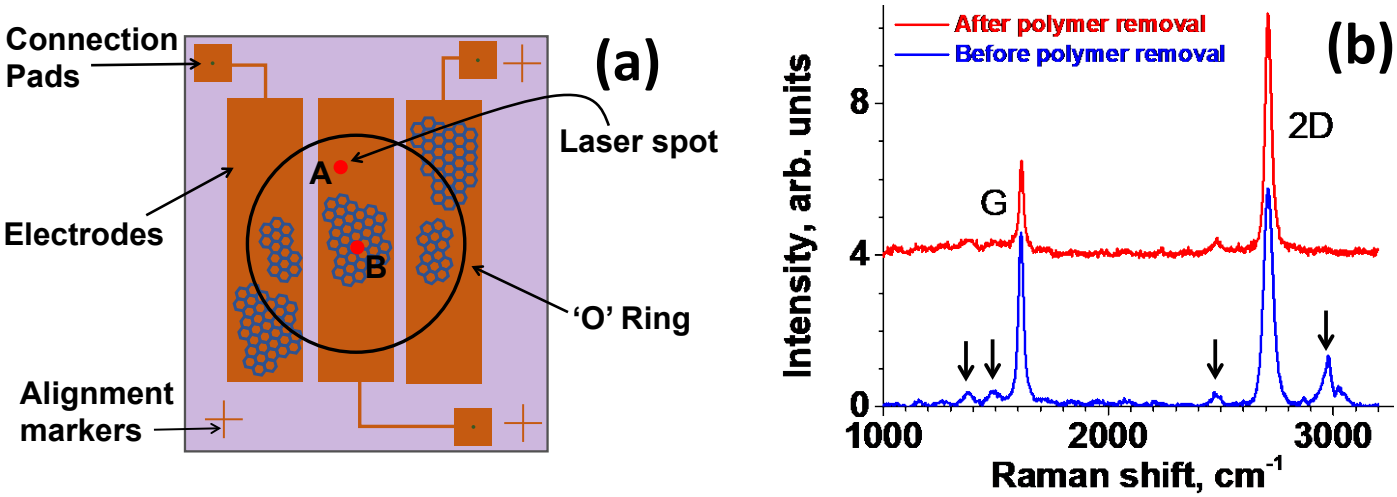

Figure 1. *Sample structure and characterization.* (a) Schematic of the chip, partially covered with one layer of graphene. The 'O' ring is the area in contact with electrolyte. A and B are typical spots of incident laser for differential reflectivity measurement. (b) Raman spectra of the graphene transferred on the electrode, before and after the removal of the polymer backing.

The structure of the electrode/electrolyte interface was measured by an in-house built differential reflectivity coupled to a potentiostat for cyclic voltammetry (CV) (Figure 2(a)). The procedure to measure differential reflectivity as a function of CV potential, E on the Au electrode (referred to as working electrode (WE)) relative to the solution, i.e., reference electrode (RE) is described in the Method Section. The instrument (in Figure 2(a)) referred to as Scanning Electrometer for Electrical Double-layer (SEED) has been described to measure local redox reaction.[19] Briefly, the intensity of reflected laser beam incident from the working electrode focused by an objective lens to ~6 μm spot was measured on a Si detector (Figure 2(a)). The location of the spot on the Au or graphene/Au electrode (i.e., A or B in Figure 1(a)) was obtained by moving the sample and visualized on a digital camera using the same objective lens (Figure 2(a)). The positions of the graphene were mapped a priori as indicated above.

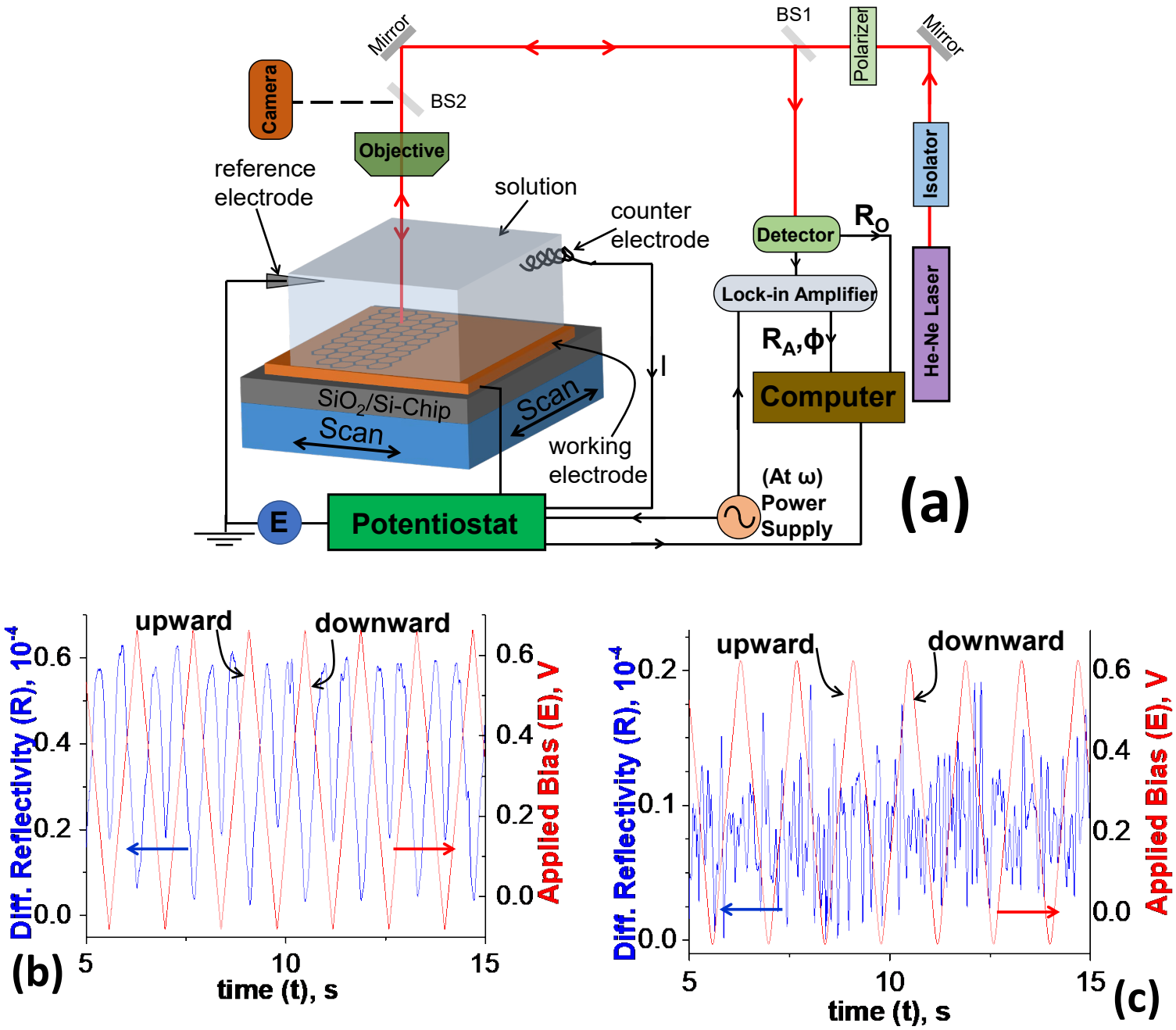

Figure 2. *Differential reflectometry of the electrode/electrolyte interface*. (a) Optical and electronic set-up of the differential interferometer. The outer Pt coated chamber holding the liquid that acts as a counter electrode (CE) is not shown. The laser beam incident on the graphene/Au was imaged by the camera of the in-line optical microscope. The incident beam R_O and the differential reflectivity, R_A at ω is measured on the detector as DC and AC signals, respectively. The latter is amplified on a lock-in-amplifier tuned at AC power supply frequency, ω. Typical raw data obtained for a segment of 30 s scan showing the R (blue, right) and E (red, right) for laser spot on, (b) Au, and (c) graphene/Au. The full scan is in SI, Figure S3.

To perform differential measurement, an additional AC potential of amplitude, A and frequency, ω = 500 Hz was applied via an external power supply on the WE during the CV ramp (Fig. 2(a)). Owing to the charge screening from the electrical double layer (EDL), the electric field emanating from the WE was confined to the interface.[20] As a result of the ion oscillation at the electrolyte/WE interface due to the AC potential caused the reflectivity of the laser beam to oscillate at ω, at an amplitude given by (see the Supporting Information (SI)[19]),

$$R = \frac{R_A}{R_O} = 4n_2 \frac{\left(k_2^2 - \langle n_{1s}\rangle^2\right)}{\left(\langle n_{1s}\rangle^2 + k_2^2\right)^2} \delta n_s \qquad (1)$$

where, δn_s is the amplitude of refractive index oscillation that is spatially averaged over the interface, R_A and R_O are the amplitude of AC intensity at ω and the incident laser intensity (i.e., DC signal), respectively, measured at the detector; $n_2 - ik_2$ is the complex refractive index of the WE; and $\langle n_{1s}\rangle$ is the spatially averaged refractive index of the solution at the interface. The signal R as a function of E was obtained by normalizing the R_A measured by a lock-in-amplifier tuned at ω with R_O. The second harmonic signal by the lock-in-amplifier was three orders of magnitude lower than the first order, thus, the system was assumed to be linear (Eq. (1)). The spatially averaged refractive index of the solution over the interface was calculated as,[19]

$$n_s = \langle n_{1s}\rangle + \frac{dn_-}{dc}\langle \delta c_s\rangle cos\omega t = \langle n_{1s}\rangle + \delta n_s cos\omega t \qquad (2)$$

where, dn_-/dc is the differential refractive index of the anion and $\langle \delta c_s\rangle$ is spatially averaged amplitude of ion oscillation in the interface. As the polarizability of cation is significantly lower, it is neglected in Eq. (2). The vibration of cations will simply add another linear term well over an order of magnitude smaller.

From Eq. (1), for complex refractive index of Au electrode at wavelength of 633 nm, $n_2 - ik_2$ is 0.21-i3.24, and $\langle n_{1s}\rangle \sim 1.5$, R is $\sim 0.65\delta n_s$. Conservatively, R of $\sim 10^{-5}$ at excellent signal-to-noise ratio can be measured (see Fig. 2(c) and 3(a) discussed below). As a result, SEED can measure δn_s of at least 10^{-5}. From Eq. (2), the amplitude of concentration oscillation, $\langle \delta c_s\rangle \sim \delta n_s/(dn/dc)$. As for NaCl solution $dn/dc \sim 10^{-2}$ M^{-1}, the sensitivity to measure $\langle \delta c_s\rangle$ is $\sim 10^{-4}$ M. For 50 mM NaCl in contact with Au electrode, the nominal concentration in the EDL, $c_o \sim 5$ M and $\zeta \sim 1$ nm.[21] Thus, the instrument is sensitive to ion displacement amplitude of $\sim(\langle \delta c_s\rangle/c_o)\zeta \sim 10^{-3}$ nm, which is similar to differential interferometry with Nomarski optics.[20a, 22] Thus, the ion oscillation amplitude sensitivity is adequate to measure the fine structure of the interface modeled by simulation studies with resolution of 10^{-2} nm,[23] and x-ray reflectivity measurements of the graphene/electrolyte fine structure.[7, 11]

The main observation of the study is the differential reflectivity, R(E), during the CV. The raw data, R corresponding to E-ramp, as a function of time, t for the laser beam spot on Au (Fig. 2(b)) compared to graphene/Au (Fig. 2(c)) on the same electrode are remarkably different. The R for the laser beam on Au (Fig. 2(b)) showed a set of distinct peaks as E ramps up and down, however, on graphene/Au the signal appeared to be completely passivated (Fig. 2(c)). (The full scans over 20 cycles are shown in SI, Fig. S3.). As the magnitude of R is proportional to the

amplitude of ion oscillation, $<\delta c_s>$ (Eq. (2)), the graphene completely cut-off the ion oscillation (Fig. 2(c)), i.e., the field emanating from the underlying Au electrode is screened by the graphene. The AC amplitude was A = 100 mV. The E is the potential with respect to the solution, i.e., the RE is considered ground. Both scans are typical of several scans obtained at different spots on the electrode by moving the beam (as indicated in Fig. 1(a)).

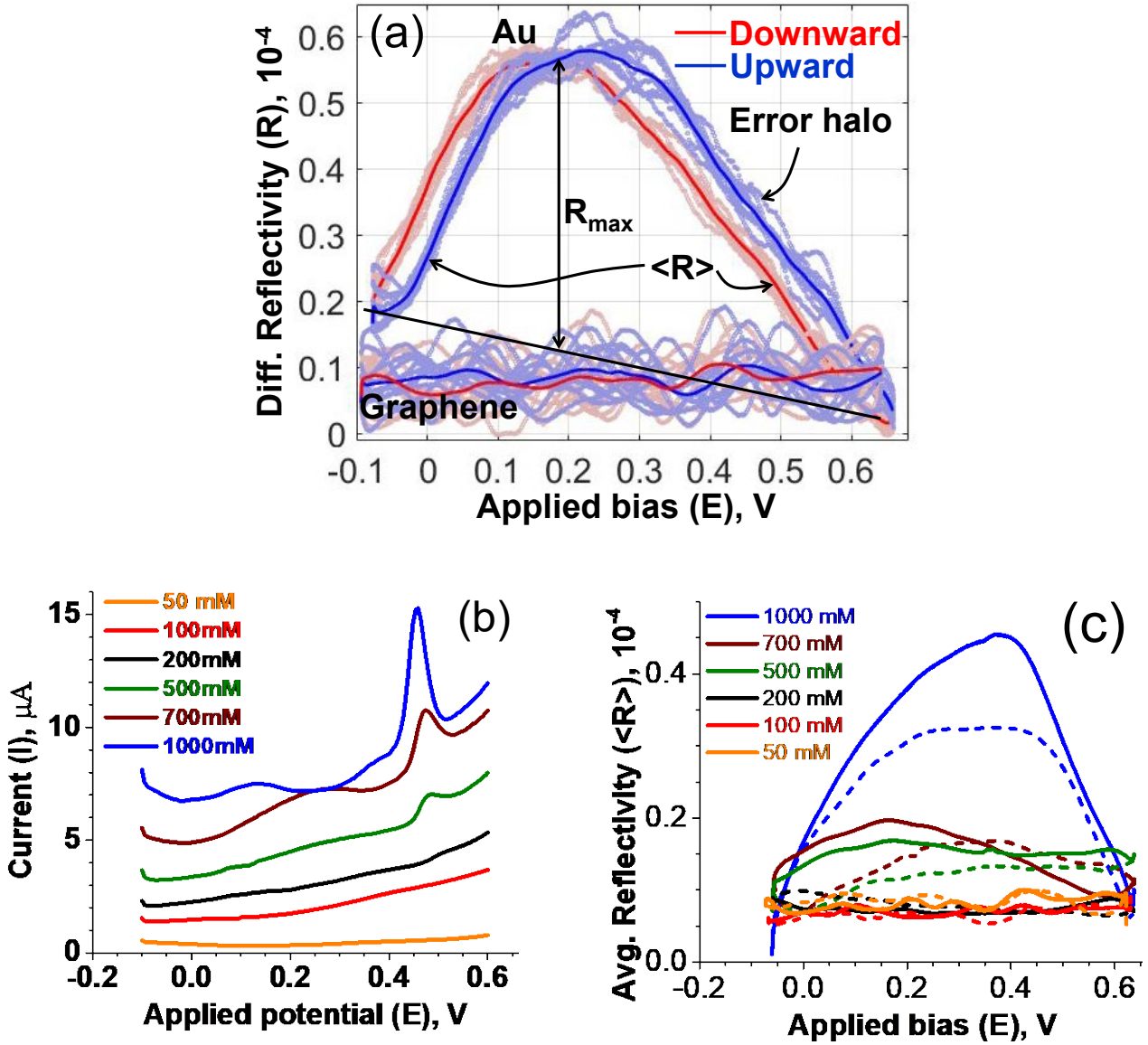

Figure 3. *Electrochemical passivation of Au Electrode by graphene monolayer.* (a) The Differential reflectivity with laser beam on the Au shows clear peaks while no significant modulation is observed on graphene/Au. The error halo is scan-to-scan variations and R_{max} is defined with respect to "downward" peak. (b) DPV at different NaCl concentration of fully coated graphene/Au electrode. (c) SEED on the same graphene/Au electrode for each of the concentrations. The downward and upward scans are dashed and solid lines, respectively. The error halo is not shown for clarity.

The solution preparation for the electrochemical analysis in presumably benign solution of NaCl interfaced with plasma cleaned Au electrode is critical. Halide ions are known to chemisorb on Au leading to a redox reaction.[24] Two steps were found to be important to eliminate the effect of Cl^- chemisorption: First, the solution was sonicated for ~30 min to remove the dissolved gases (see Methods). The resulting CV from -0.6 to 0.6 V show a significant reduction in the redox peaks (Fig. S4(a), SI). In Differential Pulse Voltammetry (DPV) where capacitance effects are suppressed and the method is more sensitive to Faradaic processes than CV, the strong redox peak at ~0.1 V is significantly suppressed on sonication (Fig. S4(b), SI). Second, on restricting the scan to -0.1 V to 0.6 V eliminated the redox peak as clearly seen in DPV (Fig. S4(c), SI). The result is a flat CV in -0.1 to 0.6 V in sonicated 50 mM NaCl solution is obtained (Fig. S4(d), SI). Thus, as will be discussed below in Fig. 4, the set of peaks observed in Fig. 2(b) is due to potential of zero charge (PZC), rather than from Cl- chemisorption. The peaks for increasing and decreasing E ramp observed in SEED (Fig. 2(b) are simply labeled upward and downward, respectively (instead of oxidation and reduction).

The complete passivation due to a single layer of graphene is better observed by plotting the average reflectivity, <R> as a function of E (Fig. 3(a)). The <R> was obtained by superimposing all the ~20 cycles of the same raw data in Fig. 2(b) and 2(c) and calculating the average R, <R>, for each E (Fig. 3(a)). The “error halo” is the cycle-to-cycle variation which was reasonably tight to obtain a peak at ~0.2 V for Au and background for graphene/Au interface. The characteristic was typical and quantitatively similar for well over 50 spots measured on well over 10 chips. The passivation of graphene on the Au electrode was very robust and always observed on all the chips for 30 electrodes. It is imperative that the observed passivation due to graphene is due to screening. A plausible cause may be low ion strength. Before, exploring a possible mechanism of screening by a monolayer of graphene, the effect of higher ion concentration is investigated and the phenomenon by alternative approaches utilized in electrochemistry was studied.

One of the electrodes was fully covered with graphene and DPV at different NaCl salt concentrations were obtained (Fig. 3(b)). Of the 12 electrodes passivated, 5 were successfully coated for full coverage. The DPV shows strong passivation by graphene up to 200 mM. A sharp redox peak at ~0.45 V is observed at higher NaCl concentrations. As DPV is sensitive to Faradic processes and relatively insensitive to non-Faradaic processes, the peak is likely due to a redox reaction that is also observed as a weak peak in the corresponding CV (Fig. S5(a), SI). The characteristics for both DPV and CV are highly reproducible and robust, i.e., changing solutions back and forth does not erase the peaks. SEED was performed on multiple spots for the same samples (Fig. 3(c)). SEED at 1 M NaCl also shows a similar peak at roughly 0.4 V (Fig. 3(c)). Consistent with DPV, in SEED, a second peak at lower bias, roughly at 0.26 V was observed at 500 mM and 700 mM (see the magnified view in Fig. S5(b), SI) and appears in 1 M NaCl as a shoulder (Fig. 3(c)). The lower bias peak in DPV ranges between 0.15 to 0.25 V for concentrations in 0.5 to 1 M range. The variations may be due to dissolved residual gases in water. This peak at lower bias, ~0.2 V, observed in DPV and SEED at high salt concentrations may be attributed to the “electronic transparency” of the underlying PZC peak of Au (Fig. 3(a)) that is enhanced at higher salt concentration. The two peaks are still not fully understood. However, it can be safely ensured that graphene monolayer completely passivates the underlying

Au electrode with no signature in CV (Fig. S5(a), SI), DPV (Fig. 3(b)) and SEED (Fig. 3(c)) for NaCl concentrations ≤200 mM. For this study, NaCl concentration was at 50 mM.

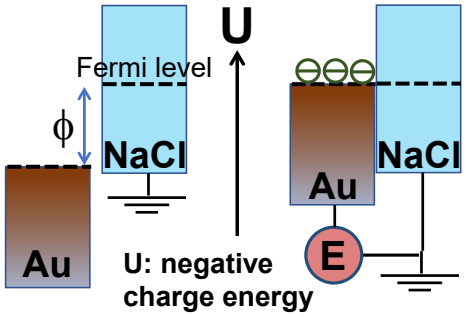

Figure 4. *The electrostatics of electrolyte/Au interface.* The (electron) energy diagram of Au/electrolyte interface before and after contact. The Fermi level of NaCl is the electrochemical potential of the solution.

The rest of the study below is in 50 mM NaCl where graphene passivates the underlying Au electrode, and no significant chemisorption occurs on Au. The peak on the Au measured by SEED at a formal potential of ~200 mV (Fig. 3(a)) is explained in terms of the charge state of the EDL. Before immersing the chip in the solution, owing to large work function of Au, the Fermi level is below by ϕ relative to the NaCl solution (Fig. 4, left). On contact, if the solution is grounded (consistent with the electrochemical circuit in Fig. 2(a)), the Fermi levels (i.e., electrochemical potentials) of the Au will rise to come to an equilibrium with the solution by adsorbing anions, Cl^- to form a negatively charged EDL (Fig. 4, right). As a result, the AC potential emanating from the Au electrode will be screened by the tight EDL (i.e., the Helmholtz layer (HL)) resulting in small oscillation of the ions and therefore the R is relatively low and flat. As potential of the Au electrode becomes positive, i.e., E > 0, the Fermi level of the Au electrode goes down and the HL is stripped causing de-screening of the AC potential leading to increase in the ion oscillation. At E = ϕ (the PZC), the HL will be completely stripped leading to a maximum in R, R_{max} (Fig. 3(a)). The potential for R_{max} in the upward and downward ramp are slightly off due to ion diffusion limitation. Analogous to the practices in electrochemistry, the average of upward and downward peaks is considered the formal potential of PZC, ϕ ~ 200 mV for 50 mM NaCl/Au interface. (To note is that the sign of applied E and PZC are consistent with the electrochemical set-up and sign of the relative Fermi level difference). Therefore, SEED directly measures PZC of the electrode surface.

The robustness of complete passivation by graphene is further confirmed by a longer scan for 5 min (SI, Fig. S6). The <R> was similar in magnitude to the 30 s scan (Fig. S3(b), SI) indicating a stable passivation behavior for A = 100 mV. The direct observation of no PZC peak by SEED on graphene/Au is in contrast to FET,[25] Hall effect,[26] and electrochemical,[27] measurements where a PZC of ~-200 mV, ~640 mV, ~-140 mV (with respect to Ag/AgCl RE) were reported, depending on the solution condition. Although, SEED is sensitive to amplitude of oscillation of ~10^{-3} nm that was reasonable to probe the EDL structure per simulation,[23] and complete passivation is observed by DPV, SEED and CV up to 200 mM of NaCl (Fig. 3(a), 3(b) and Fig.

S5(a)); the absence of the observation of PZC peak may be due to low A. Perhaps by increasing A enough field could be leaked thru the hydration layer to oscillate the ions beyond the hydration layer, i.e., in the HL, to make the observation of PZC for the graphene/Au electrode more visible.

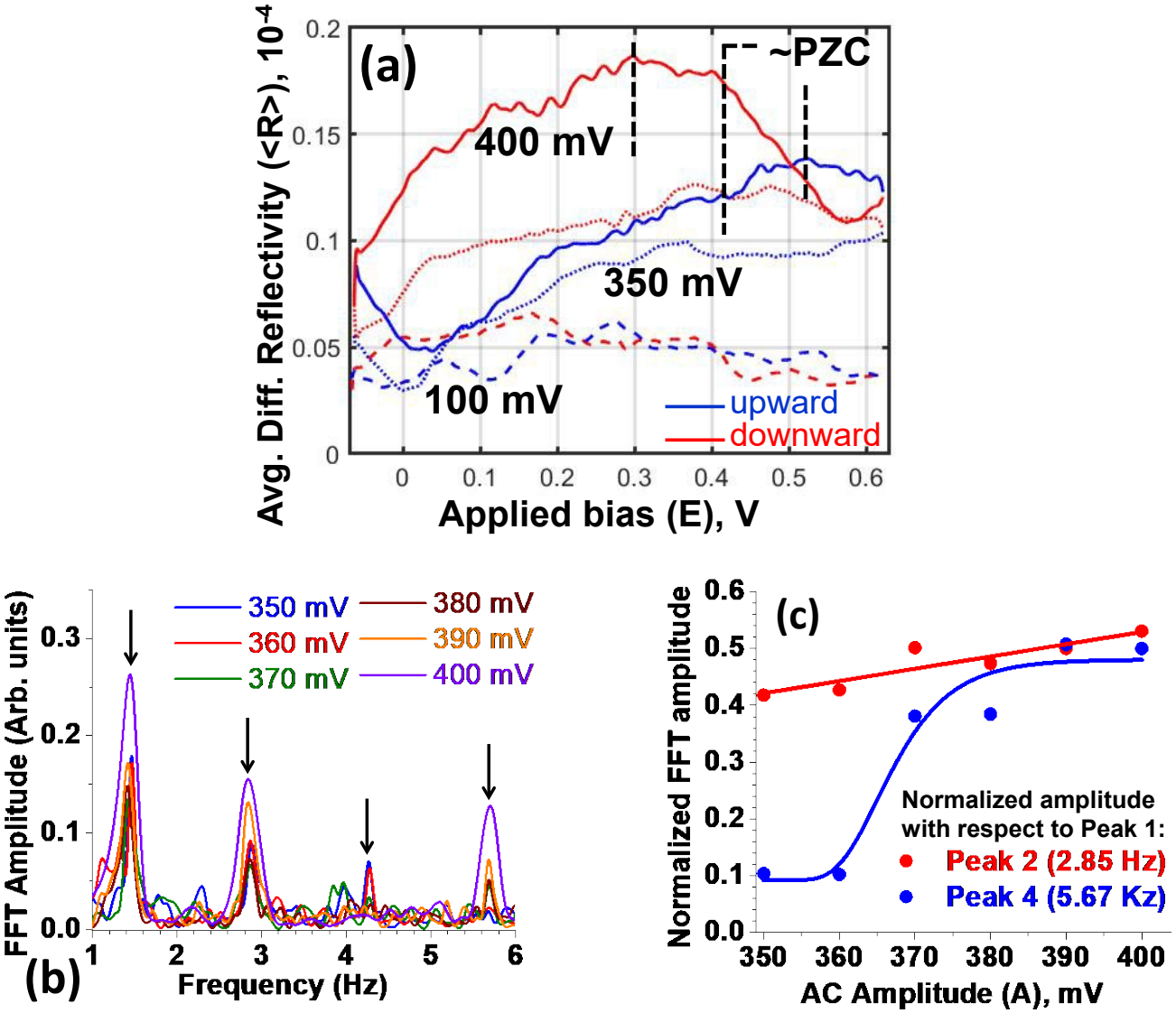

Figure 5. *Effect of AC Amplitude on reflectivity*. (a) The <R> as a function of E on the same chip for different A. The error-halo is not shown for clarity. (b) Typical Fast Fourier Transform (FFT) of R versus t of 60 s scans for each A. The FFT is smoothened by B-spline algorithm (Origin®). (c) The relative FFT amplitude of second and fourth order peak as a function of A.

Indeed, as A was systematically increased from 100 mV to 400 mV, the ion oscillation increased (Fig.5(a)). Interestingly, at higher A, a peak began to emerge at "formal potential" of ~420 mV (Fig. 5(a)). The structural periodicity was better observed by taking the Fast Fourier Transform

(MATLAB®) (Fig. 5(b)). The first order peak at frequency, f_1 ~1.4 Hz corresponds to the time period of the CV cycle, T ~ 1.4 s. Although the response on graphene/Au appears "noisy" at A = 100 mV with no periodicity (Fig. 2(c) and Fig. S3(b), SI), the harmonics in FFT are (still) observed due to capacitance effects as the ramp potential E changes direction, i.e., where dE/dt is maximum. At maximum dE/dt, the capacitance current will tend to discharge the EDL leading to deeper penetration of the electric field emanating from the electrode. Because the CV ramp changes direction twice in a cycle, $f_1 \sim 2/T$. The higher order peaks were due to the electrochemical peaks. As A increases the 2nd and 4th order harmonics corresponding to capacitance and PZC peaks, respectively become stronger (Fig. 5(b)). The 2nd order at f_2 ~ 2.8 Hz increases linearly at a small slope illustrating that the ion vibrations gradually become stronger as A increases due to the periodic CV ramp (Fig. 5(c)). However, the 4th order rapidly increases for E above 360 mV indicating a (sharp) threshold to disrupt the hydration layer exposing the emanating electric field. To note is that the relative FFT plotted in Fig. 5(c) are based on the raw peak amplitudes (Fig. S7, SI) rather than the smoothened spectrum in Fig. 5(b). As the sample should be completely passivate by graphene as indicated by CV, DPV and SEED at 50 mM NaCl, the origin of ~420 mV peak is not a redox (observed in DPV) but effective PZC of the graphene/Au electrode after the hydration layer is disrupted. Subsequently, the ~420 mV peak in SEED will be referred to as (effective) PZC of graphene/Au electrode.

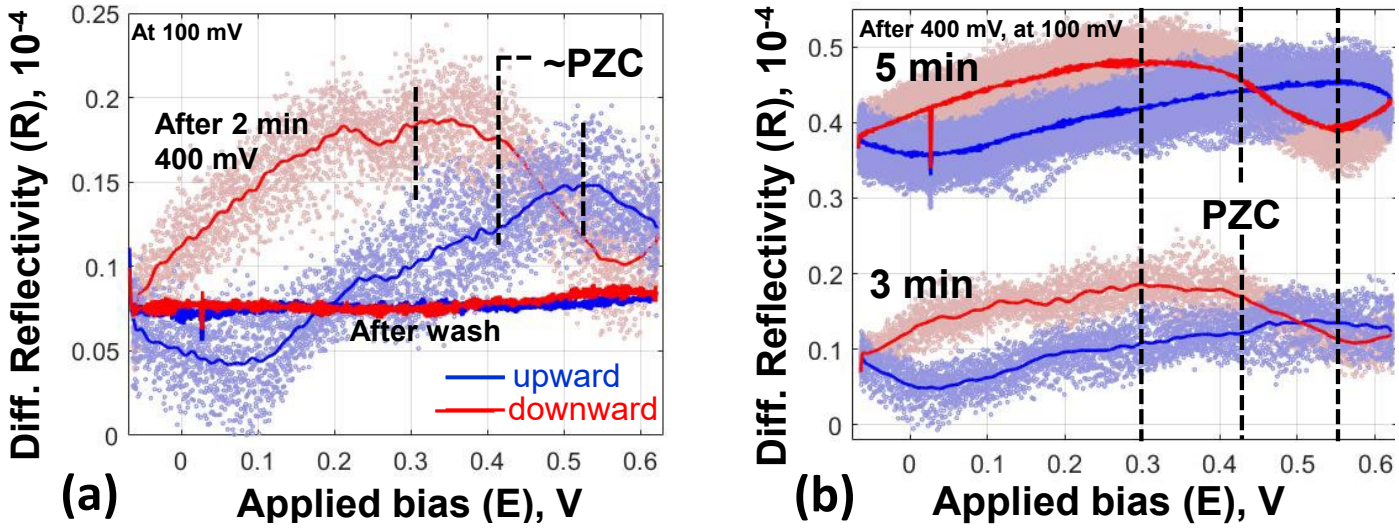

Figure 6. *Mechanical stability of the graphene/Au interface at a spot on the electrode*. (a) The R as a function of E at A = 100 mV measured after 400 mV exposure and subsequent wash. (b) The behavior of two electrodes on the same chip exposed for 3 and 5 min.

On longer exposure to 400 mV AC potential for 120 s and measuring at A = 100 mV, the ~420 mV peak was more defined (Fig. 6(a)) compared to the peak in Fig. 5(a)). However, the magnitude of R_{max} did not change significantly. On flushing the sample with 50 mM NaCl solution without removing the sample from the optical set-up, on the same graphene/Au spot, the peak was completely erased leading to passivation (Fig. 6(a)). This was repeated over several

400 mV exposure and wash cycles with no degradation of the signal. Other two electrodes on the same chip were exposed to 400 mV for (same) 3 and 5 mins respectively and SEED was performed at 100 mV (Fig. 6(b)). Although the background (i.e., baseline) vibrations increased, the R_{max} was nominally unchanged and the PZC remained constant at about ~420 mV. Again, the process was reversible by a simple washing step. Thus, the reversibility of the peak at ~420 mV indicated that no degradation of graphene occurred, but it was due to mechanical rupture of the hydration layer. It was also discovered that once the interface is disrupted at 400 mV it does not relax back spontaneously even after 2 hrs. Washing was necessary. Thus, from the slow kinetics of disruption (i.e., in minutes) and reformation (in over hours), the hydration layer is perhaps a "gel-like" layer with slow dynamics to recover.

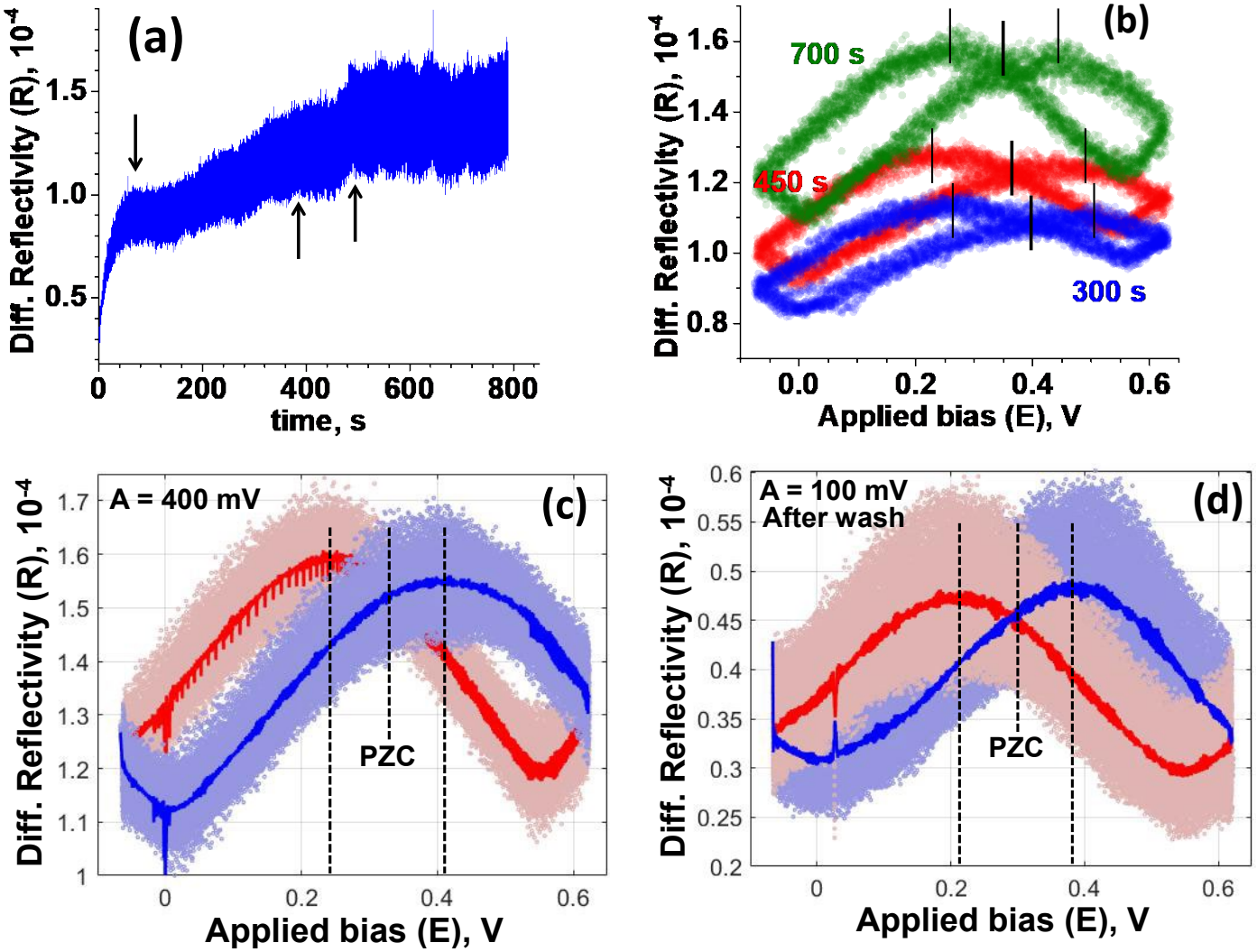

Figure 7. *Permanent degradation of the graphene/Au structure*. (a) A long exposure to CV at A = 400 mV. The CV ramp from -0.1 to 0.6 V is not shown for clarity. (b) R(E) for 10 s scan segments at three different stages of the 400 mV exposure. The solid line indicates the maxima (light) and the PZC (heavy) location of E. (c) The average response in the plateau region from t = 480 to 790 s. (d) The average response at 100 mV measured over 5 min scan after washing the sample.

Although, unlike the behavior at long exposure at A = 100 mV (Fig. S6, SI), the signal for longer exposure at 400 mV for 5 mins increased monotonically with peaks getting sharper and significantly larger over time (Fig. S8, SI). However, after the exposure, at A = 100 mV the signal was similar to Fig. 6(b) and reversible on wash. On continued exposure for ~800 s, at A = 400 mV both the baseline and range of modulation continues to increase as signified by the "band" of the R (Fig. 7(a)). Up to 300 s the PZC remains about 400 to 420 mV (Fig. 7(b), blue) which is consistent with Fig. 6(b). Above 300 s the formal potential of the PZC gradually shifts towards lower values. At 450 s and 700 s the effective PZC is ~370 mV and ~350 mV, respectively (Fig. 7(b)). After the complete exposure for 800 s, the PZC is at ~320 mV (Fig. 7(c)). After flushing with 50 mM NaCl without moving the sample and performing SEED at A = 100 mV the change was not reversible, i.e., the strong PZC peaks at ~320 mV remained (Fig. 7(d)). Thus, for long exposure at 400 mV beyond 300 s the graphene was eventually damaged exposing a small amount of the underlying Au causing a shift towards PZC of Au at ~0.2 V (Fig. 3(a)). From the gradual shift in PZC, it appears that the electric field influenced degradation is a gradual and slow process. Perhaps, the degradation is impeded due to the slow kinetics of disruption of the hydration layer.

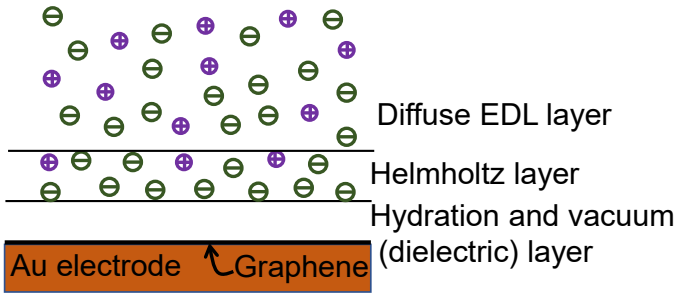

Figure 8. electrolyte/graphene interface. An idealized schematic of the stratified structure of electrolyte/graphene/Au interface.

To visualize and explain the remarkable passivation of electric field by a monolayer of graphene attributed to the hydration layer, and its disruption, an idealized interfacial structure based reported simulation and experimental studies may be considered (Fig. 8).[4a, 7, 23] Simulation studies show that the hydration layer is a hydrophobic bilayer of water with no dangling hydrogen bonds.[4a, 9a] It hydration layer forms past the ~1 nm thick "vacuum" layer at the interface,[7] and is ~0.3 nm thick.[23a] A HL is formed with strong attraction of Cl^- within 0.4 nm and week layers of Na^+ within the first 0.5 nm.[23a] As a result, within ~2.5 nm the potential is completely screened by, (a) the compensating ions in the HL, and (b) the dielectric polarization of the water molecules in the hydration layer.[23b] Importantly, the hydration layer substantially weakens the electric field to maintain the charge in the HL at all potentials, E in ±0.6 V. Unlike the EDL on Au where Cl^- strongly adsorbs on the electrode but does not completely screens the electric field and is highly mobile, for graphene, the field on graphene is completely screened because of the (opposing) displacement electric field in the hydration layer. Because the hydration layer is highly cross-linked gel-like thin film it is fairly stable but suddenly begins to rupture for A > 360 mV.

CONCLUSIONS

The interfacial properties of Au electrode covered with monolayer of graphene in 50 mM NaCl solution is studied by differential reflectivity. The reflectivity measurement during cyclic voltammetry allowed an insight in the unusual electrostatic properties of spontaneously forming hydration layer at graphene/electrolyte interface due to the hydrophobic and conducting nature of graphene. The surprising aspect of the study were three: First, the strong displacement field due to the high dielectric constant of the hydration layer substantially weakened the potential to maintain the charge in the HL leading to significant screen of the electric field within a few nm. Second, for AC potential above 360 mV, the hydration layer becomes mechanically unstable and begins to break down exposing the graphene/Au electrode to obtain an effective PZC of ~420 mV. The ~220 mV shift relative to the PZC of underlying Au is quantitatively consistent with the ~200 mV shift in work function of graphene/Au relative to Au in vacuum.[17a] Third, the hydration layer is highly and strongly hydrogen bonded to withstand high AC potential. However, it abruptly starts to rupture at A > 360 mV and has a very slow healing kinetics, i.e., does not recover in 2 hrs. The slow kinetics indicates the hydration layer may be highly cross linked thin-film gel. The observation is likely to play a crucial role in our understanding and designing energy devices such as supercapacitors and electrochemical sensors using graphene electrodes.

METHODS

Deposition of Graphene on a chip with Au electrode. The sample was a ~200 μm thick Si chip passivated with ~1 μm thermal oxide (SiO_2). The chip was 1 by 1 cm. The chip had three 2 x 8 mm Au electrodes of thickness ~100 nm deposited by standard lithography using ~50 nm Cr as adhesion layer (see Fig. 1(a)). "Easy Transfer" Graphene was purchased from Graphenea, Inc. This graphene sample was a single layer thick, with a nanoporous polymer protective layer. The graphene was cut with a steel blade and was allowed to float on DI water until picked up by a gold-silica chip. The chip was then heat treated at 150°C on a hotplate for an hour and stored in a vacuum overnight to remove water from the sample. The next day, the protective polymer was removed by heat treating the sample at 150°C, soaked in pure acetone, and then in pure isopropyl alcohol, each for one hour, resulting in a single layer of graphene on the Au electrode as schematically shown in Fig. 1(a). Prior to deposition, the chip was cleaned with 25 mTorr, 60 W, O_2 plasma for 4 min and H_2 plasma for 2 mins. The typical size of the graphene flake was roughly 2 mm^2.

Raman spectroscopy characterization of Graphene on Au electrode. The primary tool to characterize the structure of the graphene deposited on the Au electrode was Raman spectroscopy (Renishaw inVia^{TM} Confocal Raman microscope). The Raman spectrum was measured using an Argon ion laser (λ = 514 nm). The spectra were acquired using a 50X lens with an accumulation speed of 1.0 s per position and beam diameter of 2 μm.

Differential reflectometer. The differential reflectometer based on Nomarski optics was built in-house.[19, 22] The conceptual detail of the instrument is briefly described below in the Results

and Discussion (see Fig. 2(a)). Briefly, the chip with graphene on the Au electrode was mounted in a Pt plated stainless steel chamber holding ~0.3 mL solution of 50 mM NaCl. Importantly, the solution of NaCl were made in water degassed by 15 min sonication (ELMA ultrasonic P60H on degas mode at 37kHz). The chamber at the bottom makes a hermetic seal contact with the chip using a ~5 mm O-ring (Fig. 1(a)). The area in the 'O' ring is in contact with the solution. The circuitry allows connection to the electrode via the connecting pads from outside the liquid using Au plated pogo pins (IDI Corp.) (Fig. 1(a)). An ~7 mm quartz window at the top of the chamber allows a 2 mW He-Ne laser beam to perform reflectivity measurement. The ~6 μm diameter laser beam is positioned using an inline microscope with a digital camera. Differential reflectometry is performed by positioning the beam either on the Au electrode (spot A) or graphene/Au (spot B) (Fig. 1(a)).

Cyclic voltammetry. CV was performed during differential interferometry using a potentiostat (Metrohm USA, Autolab PGSTAT303N/FRA32) in a classic three-electrode configuration. The chip is the working electrode (WE) connected via the connecting pads (in Fig. 2(b)). A port was designed in the sample chamber to insert a Ag/AgCl reference electrode (RE). The Pt plated sample chamber holding the fluid (not shown in Fig. 2(a)) was the counter electrode (CE). A "V-shaped" ramp was applied between the RE and WE with a time-period of ~1.4 s. For differential interferometry, an additional AC potential was applied to WE at a frequency of 500 Hz and an amplitude ranging from 100 to 400 mV. To note is that the frequency of CV potential is significantly slower than frequency of AC potential so that the differential reflectivity corresponds to the CV potential. The CV characterizations were performed at a ramp rate of 25 mV/s. The range of the scans are discussed in the text above and shown in the figures.

Differential pulse voltammetry. DPV was performed with 0.005 V step size, 0.025 V modulation amplitude, 0.1 s modulation time and 0.5 s interval time. The range of the scans are discussed in the text above and shown in the figures.

ASSOCIATED CONTENT

Supporting Information

Supporting information contains Raman microscopy data, raw data of differential reflectivity under various conditions, and fast Fourier spectrum.

AUTHOR INFORMATION

ARS, KK, JAA conducted the experiments. All authors contributed towards planning the experiment and preparing the manuscript.

CONFLICT OF INTEREST

Authors have no financial or commercial conflict of interest.

REFERENCES

[1] a) M. F. El-Kady, V. Strong, S. Dubin, R. B. Kaner, *Science* **2012**, *335*, 1326-1330; b) H. Ji, X. Zhao, Z. Qiao, J. Jung, Y. Zhu, Y. Lu, L. L. Zhang, A. H. MacDonald, R. S. Ruoff, *Nature Communications* **2014**, *5*, 3317; c) Y. W. Zhu, S. Murali, M. D. Stoller, K. J. Ganesh, W. W. Cai, P. J. Ferreira, A. Pirkle, R. M. Wallace, K. A. Cychosz, M. Thommes, D. Su, E. A. Stach, R. S. Ruoff, *Science* **2011**, *332*, 1537-1541.

[2] a) F. Chen, Q. Qing, J. Xia, N. Tao, *Chemistry – An Asian Journal* **2010**, *5*, 2144-2153; b) A. Das, S. Pisana, B. Chakraborty, S. Piscanec, S. K. Saha, U. V. Waghmare, K. S. Novoselov, H. R. Krishnamurthy, A. K. Geim, A. C. Ferrari, A. K. Sood, *Nat. Nanotechnol.* **2008**, *3*, 210-215; c) W. Fu, L. Feng, G. Panaitov, D. Kireev, D. Mayer, A. Offenhäusser, H.-J. Krause, *Science Advances* **2017**, *3*, e1701247; d) L. J. A. Macedo, R. M. Iost, A. Hassan, K. Balasubramanian, F. N. Crespilho, *ChemElectroChem* **2019**, *6*, 31-59.

[3] S. Gim, K. J. Cho, H.-K. Lim, H. Kim, *Scientific Reports* **2019**, *9*, 14805.

[4] a) A. Akaishi, T. Yonemaru, J. Nakamura, *ACS Omega* **2017**, *2*, 2184-2190; b) Y. J. Shin, Y. Wang, H. Huang, G. Kalon, A. T. S. Wee, Z. Shen, C. S. Bhatia, H. Yang, *Langmuir* **2010**, *26*, 3798-3802.

[5] Z. Li, Y. Wang, A. Kozbial, G. Shenoy, F. Zhou, R. McGinley, P. Ireland, B. Morganstein, A. Kunkel, S. P. Surwade, L. Li, H. Liu, *Nat. Mater.* **2013**, *12*, 925-931.

[6] K. A. B. Dill, S. Bromberg, *Molecular Driving Forces: Statistical Thermodynamics in Chemistry and Biology*, Garland Science, New York, NY, **2003**, Chapter 21, p. 401.

[7] H. Zhou, P. Ganesh, V. Presser, M. C. F. Wander, P. Fenter, P. R. C. Kent, D.-e. Jiang, A. A. Chialvo, J. McDonough, K. L. Shuford, Y. Gogotsi, *Physical Review B* **2012**, *85*, 035406.

[8] M. B. Hillyer, B. C. Gibb, *Annual Review of Physical Chemistry* **2016**, *67*, 307-329.

[9] a) M. Pykal, M. Langer, B. Blahová Prudilová, P. Banáš, M. Otyepka, *The Journal of Physical Chemistry C* **2019**, *123*, 9799-9806; b) J. Dočkal, F. Moučka, M. Lísal, *The Journal of Physical Chemistry C* **2019**, *123*, 26379-26396; c) H. Yang, Z. Bo, J. Yang, J. Kong, X. Chen, J. Yan, K. Cen, *ChemElectroChem* **2017**, *4*, 2966-2974; d) R. P. Misra, D. Blankschtein, *Langmuir* **2021**, *37*, 722-733; e) M. Imai, Y. Yokota, I. Tanabe, K. Inagaki, Y. Morikawa, K.-i. Fukui, *Physical Chemistry Chemical Physics* **2020**, *22*, 1767-1773.

[10] T. Utsunomiya, Y. Yokota, T. Enoki, K.-i. Fukui, *Chemical Communications* **2014**, *50*, 15537-15540.

[11] R. Hayashi, N. Hoshi, O. Sakata, M. Nakamura, *The Journal of Physical Chemistry C* **2018**, *122*, 7795-7800.

[12] a) Y. Huang, X. Chen, M. Q. Zhang, *Journal of Materials Science* **2014**, *49*, 3025-3033; b) Z. Xu, Z. Ao, D. Chu, A. Younis, C. M. Li, S. Li, *Scientific Reports* **2014**, *4*, 6450.

[13] S. R. Accordino, J. M. M. d. Oca, J. A. R. Fris, G. A. Appignanesi, *The Journal of Chemical Physics* **2015**, *143*, 154704.

[14] A. V. Prydatko, L. A. Belyaeva, L. Jiang, L. M. C. Lima, G. F. Schneider, *Nature Communications* **2018**, *9*, 4185.

[15] a) K. Ma, X. Wang, Y. Cui, F. Lin, C. Deng, H. Shi, *Chemical Physics Letters* **2017**, *677*, 137-142; b) M. D. Stoller, C. W. Magnuson, Y. W. Zhu, S. Murali, J. W. Suk, R. Piner, R. S. Ruoff, *Energy Environ. Sci.* **2011**, *4*, 4685-4689; c) J. L. Xia, F. Chen, J. H. Li, N. J. Tao, *Nat. Nanotechnol.* **2009**, *4*, 505-509.

[16] a) J. Rafiee, X. Mi, H. Gullapalli, A. V. Thomas, F. Yavari, Y. Shi, P. M. Ajayan, N. A. Koratkar, *Nat. Mater.* **2012**, *11*, 217-222; b) C.-J. Shih, Q. H. Wang, S. Lin, K.-C. Park, Z. Jin, M. S. Strano, D. Blankschtein, *Physical Review Letters* **2012**, *109*, 176101.
[17] a) S. M. Song, J. K. Park, O. J. Sul, B. J. Cho, *Nano Letters* **2012**, *12*, 3887-3892; b) K. Xu, C. F. Zeng, Q. Zhang, R. S. Yan, P. D. Ye, K. Wang, A. C. Seabaugh, H. G. Xing, J. S. Suehle, C. A. Richter, D. J. Gundlach, N. V. Nguyen, *Nano Letters* **2013**, *13*, 131-136.
[18] A. C. Ferrari, D. M. Basko, *Nat. Nanotechnol.* **2013**, *8*, 235-246.
[19] R. Tevatia, A. Prasad, R. F. Saraf, *Analytical Chemistry* **2019**, *91*, 10501-10508.
[20] a) G. Singh, D. Moore, R. F. Saraf, *Analytical Chemistry* **2009**, *81*, 6055-6060; b) G. Singh, R. F. Saraf, *Journal of Physical Chemistry B* **2006**, *110*, 12581-12587.
[21] J. N. Israelachvili, *Intermolecular and Surface Forces (Third Edition)*, Academic Press, Boston, **2011**.
[22] S.-W. Lee, R. F. Saraf, *Biosensors and Bioelectronics* **2014**, *57*, 41-47.
[23] a) D. J. Cole, P. K. Ang, K. P. Loh, *The Journal of Physical Chemistry Letters* **2011**, *2*, 1799-1803; b) G. Jiang, C. Cheng, D. Li, J. Z. Liu, *Nano Research* **2016**, *9*, 174-186.
[24] O. M. Magnussen, *Chemical Reviews* **2002**, *102*, 679-726.
[25] M. Dankerl, M. V. Hauf, A. Lippert, L. H. Hess, S. Birner, I. D. Sharp, A. Mahmood, P. Mallet, J.-Y. Veuillen, M. Stutzmann, J. A. Garrido, *Advanced Functional Materials* **2010**, *20*, 3117-3124.
[26] M. A. Brown, M. S. Crosser, A. C. Ulibarri, C. V. Fengel, E. D. Minot, *The Journal of Physical Chemistry C* **2019**, *123*, 22706-22710.
[27] J. Poon, C. Batchelor-McAuley, K. Tschulik, R. G. Compton, *Chemical science* **2015**, *6*, 2869-2876.

Supporting Information

Electrostatics of Single Monolayer Graphene Coated Metal Electrode in Electrolyte

Akshat R. Saraf[1], Kamran Keramatnejad[2], Jennifer A. Arcila[3], Ravi F. Saraf[3,*]

[1]Department of Nanoengineering, University of California at San Diego, La Jolla, CA 92093; [2]Vajra Instrument, Lincoln, NE 58512; [3]Department of Chemical and Biomolecular Engineering, University of Nebraska – Lincoln, NE 68588.

Section 1: Raman Spectrum and Optical Microscopy

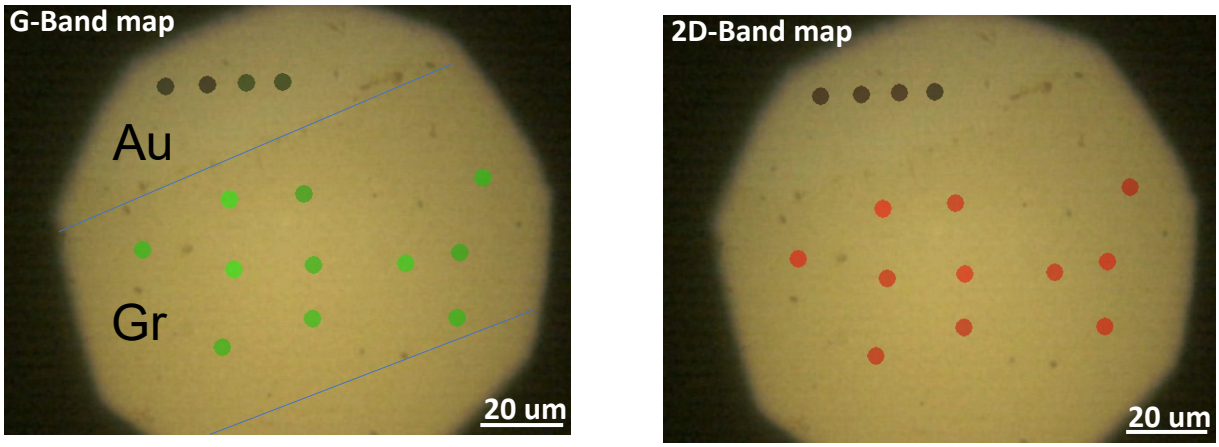

Fig. S1. Optical microscope image on the Raman microscope of Graphene deposited on the Au electrode. The dots are where the Raman spectrum was taken. No G or 2D peaks were observed on Au. The line indicating the is boundary of graphene is to guide the eye.

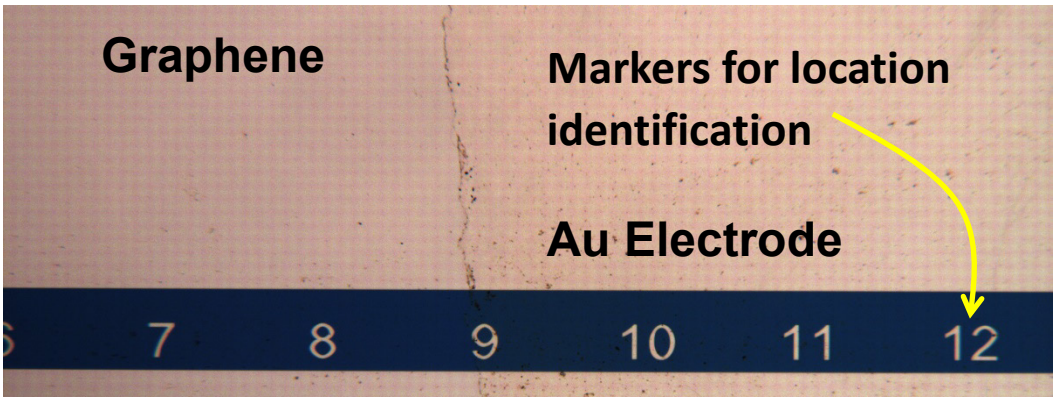

Fig. S2. Optical microscope image of Graphene deposited on the Au electrode. The numerical markers patterned on the Au electrode is to help locate the approximate position of the graphene crystals on the electrode.

Section 2: Raw data for differential reflectivity

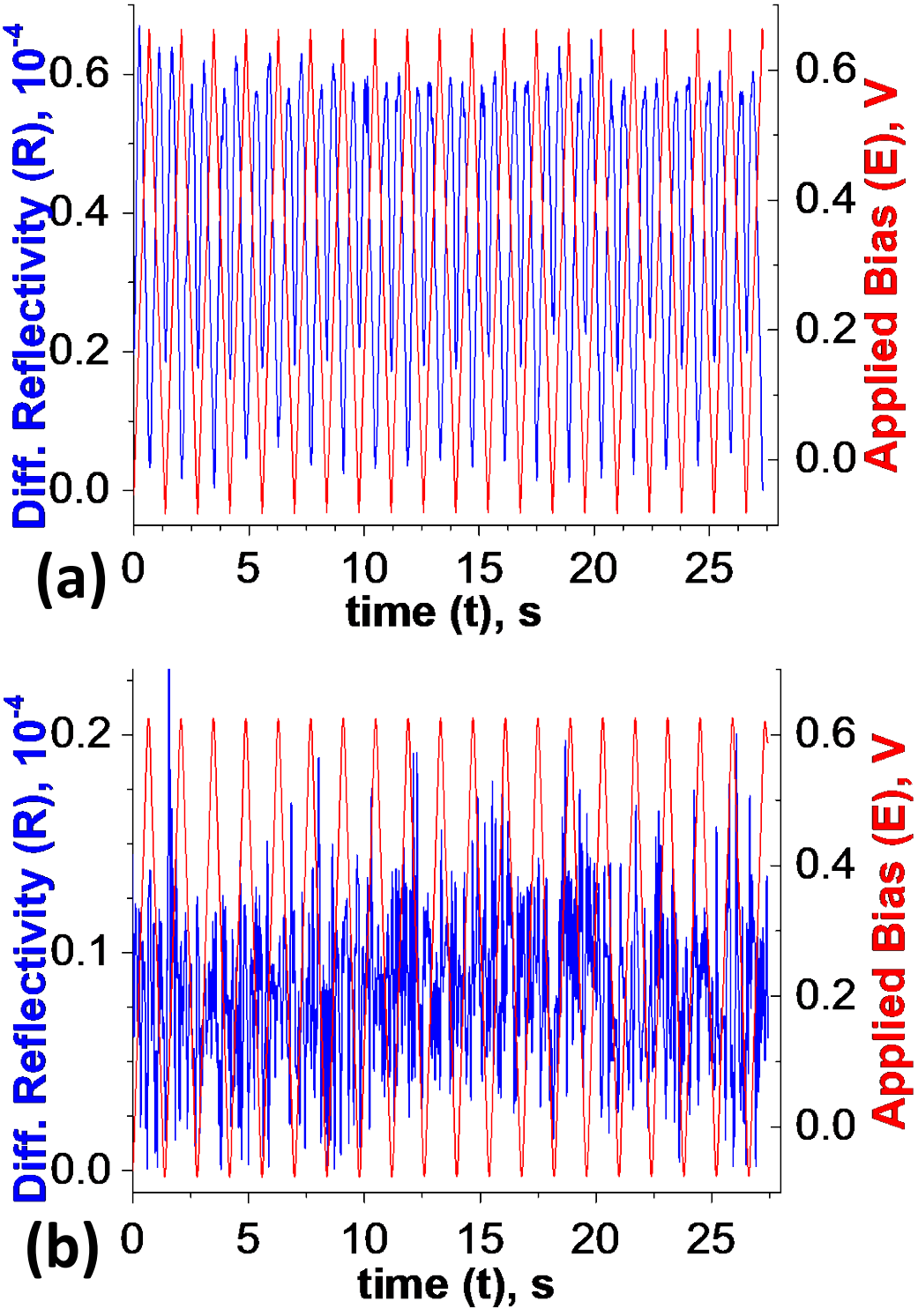

Fig. S3. Raw data from SEED. Raw data for ~60 s scan showing the R (blue, right) and E (red, right) for laser spot on, (a) Au, and (b) graphene/Au.

Section 3: Electrochemical characterization of Au electrode after plasma cleaning

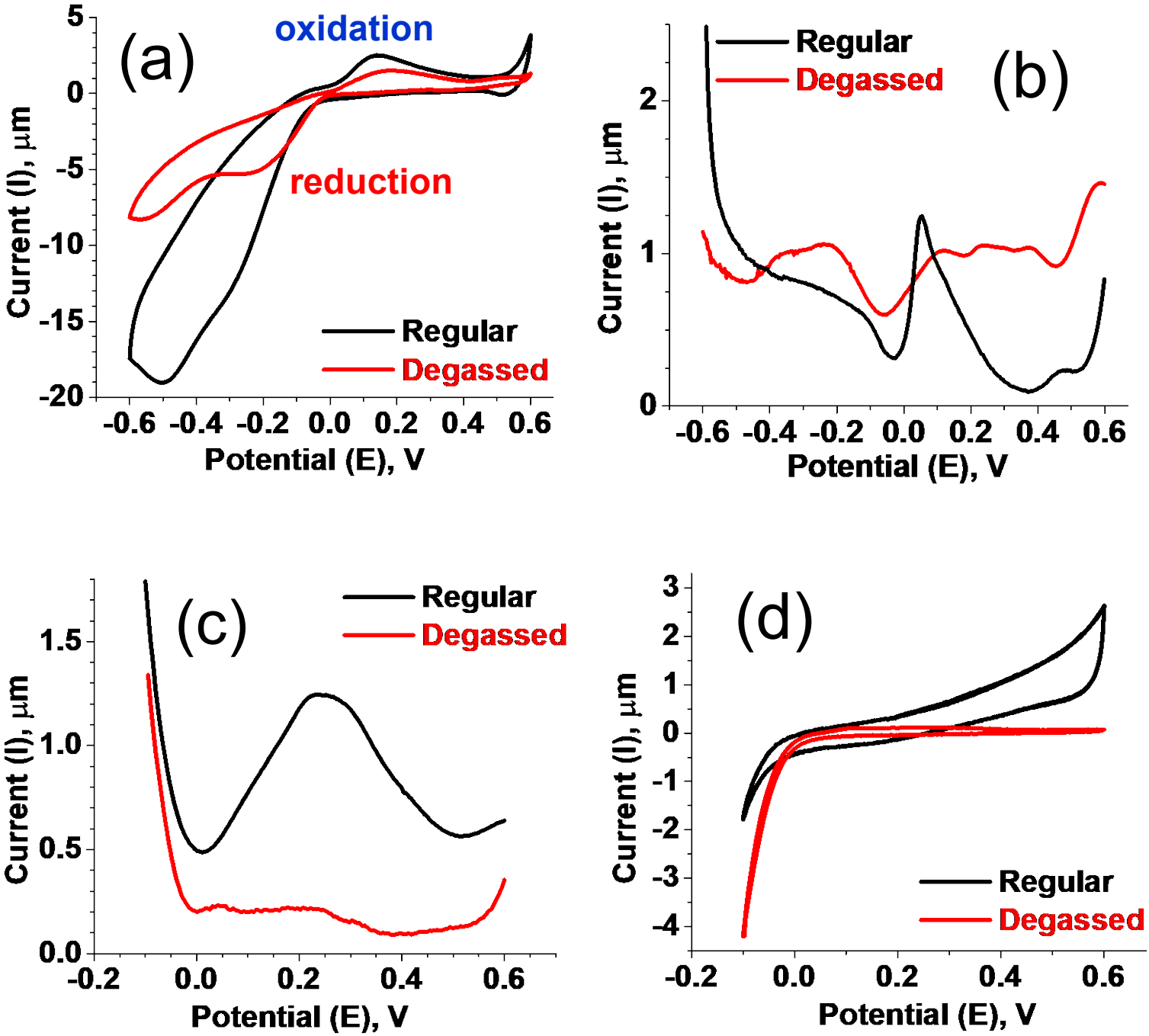

Fig. S4. Fig. S4. Effect of degassing and potential range on the electrochemical activity at Au interface to 50 mM NaCl solution in DI water is studied. (a) CV from -0.6 to 0.6 V shows clear oxidation and reduction peaks at roughly, 0.2 V and -0.2 V, respectively. However, degassing significantly reduces the current. (b) The corresponding DPV showed a clear redox peak at ~0.05 V in that was eliminated on sonicating, degassing the solution. (c) DPV, and (d) CV of 50 mM NaCl in contact with pristine Au in a range from -0.1 to 0.6 V. Both the CV and DPV in indicate that the electrochemical activity is significantly reduced due to sonication. Importantly, no redox is observed in DPV, and CV is nominally flat, for -0.1 to 0.6 V range, after the sonication process.

Section 4: Effect of NaCl concentration on graphene/Au electrode

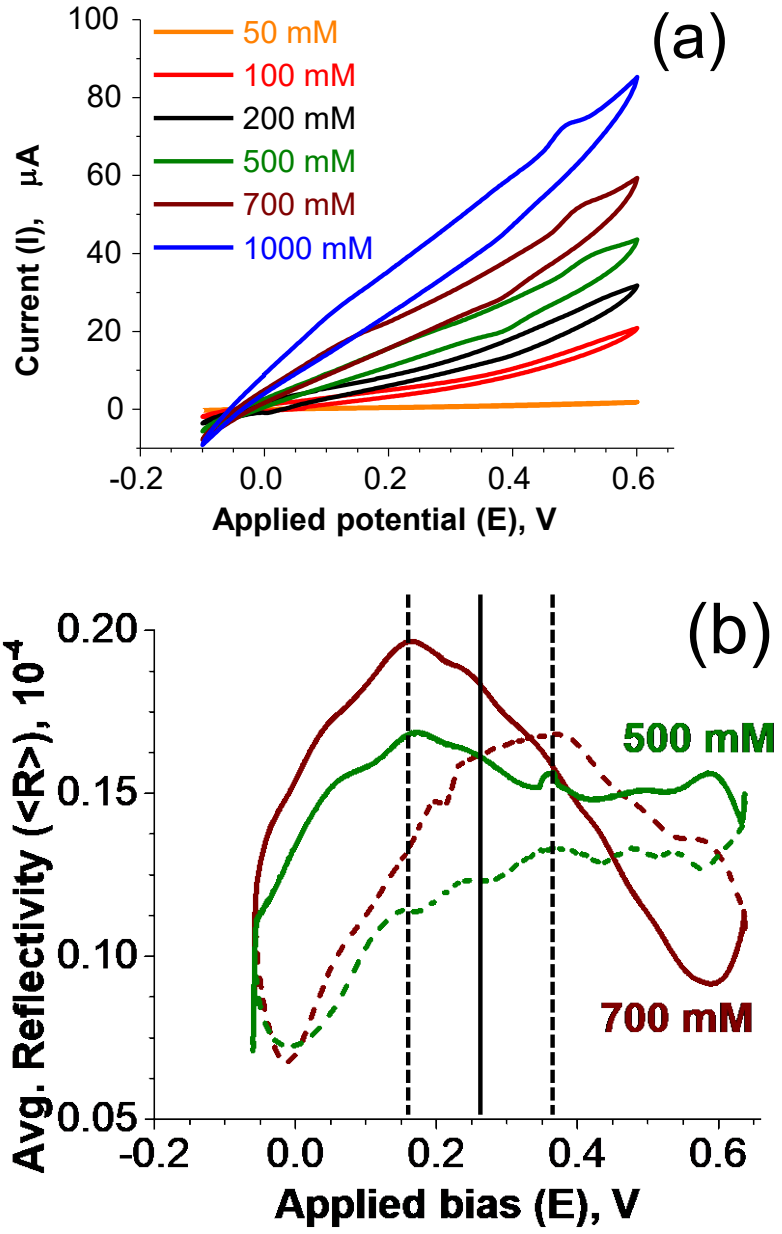

Fig. S5. (a) CV at different NaCl concentration of fully coated graphene/Au electrode. The CV is on the same sample as the DPV shown in Fig. 3(b) in the main paper. (b) SEED for 500 and 700 mM NaCl. Same as Fig. 3(c) in main paper with expanded y-axis to clearly show the upward and downward peaks.

Section 5: Differential reflectivity for long time for A = 100 mV

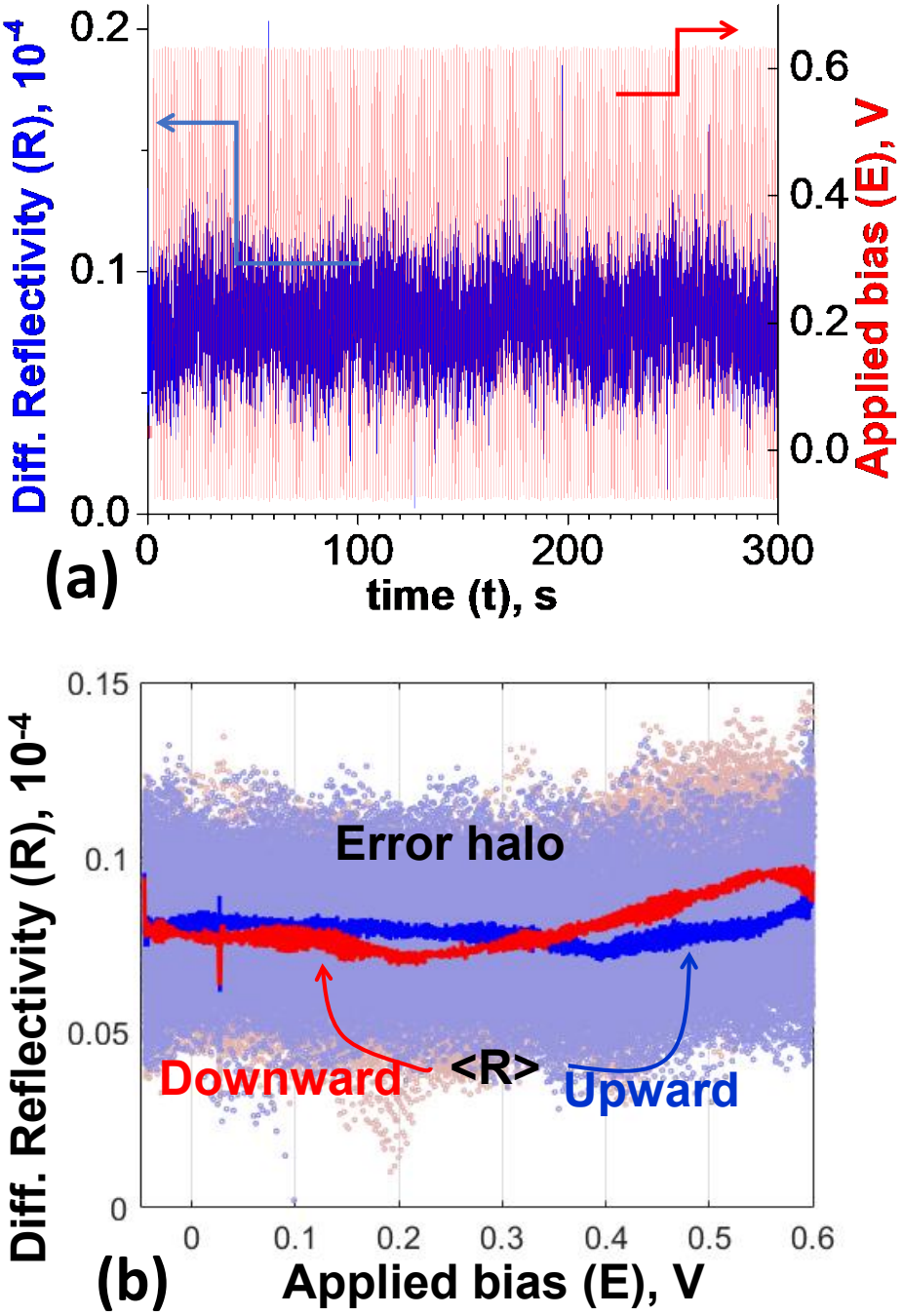

Fig. S6. SEED Response on graphene/Au electrode for 5 mins. (a) Raw data. (b) <R> as a function of E corresponding to the raw data. The amplitude of AC potential was 100 mV.

Section 6: Fast Fourier Transform of the R as a function t

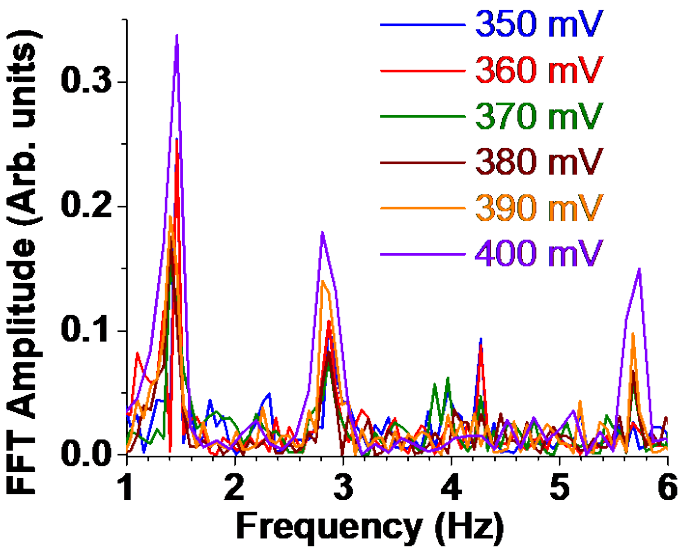

Fig. S7. Fast Fourier Transform of the raw data of R(t) measured for A = 350 to 400 mV. The raw data corresponds to some of the E versus <R> responses shown in Fig. 4.

Section 7: Differential Reflectivity for a long exposure at A = 400 mV on graphene/Au spot

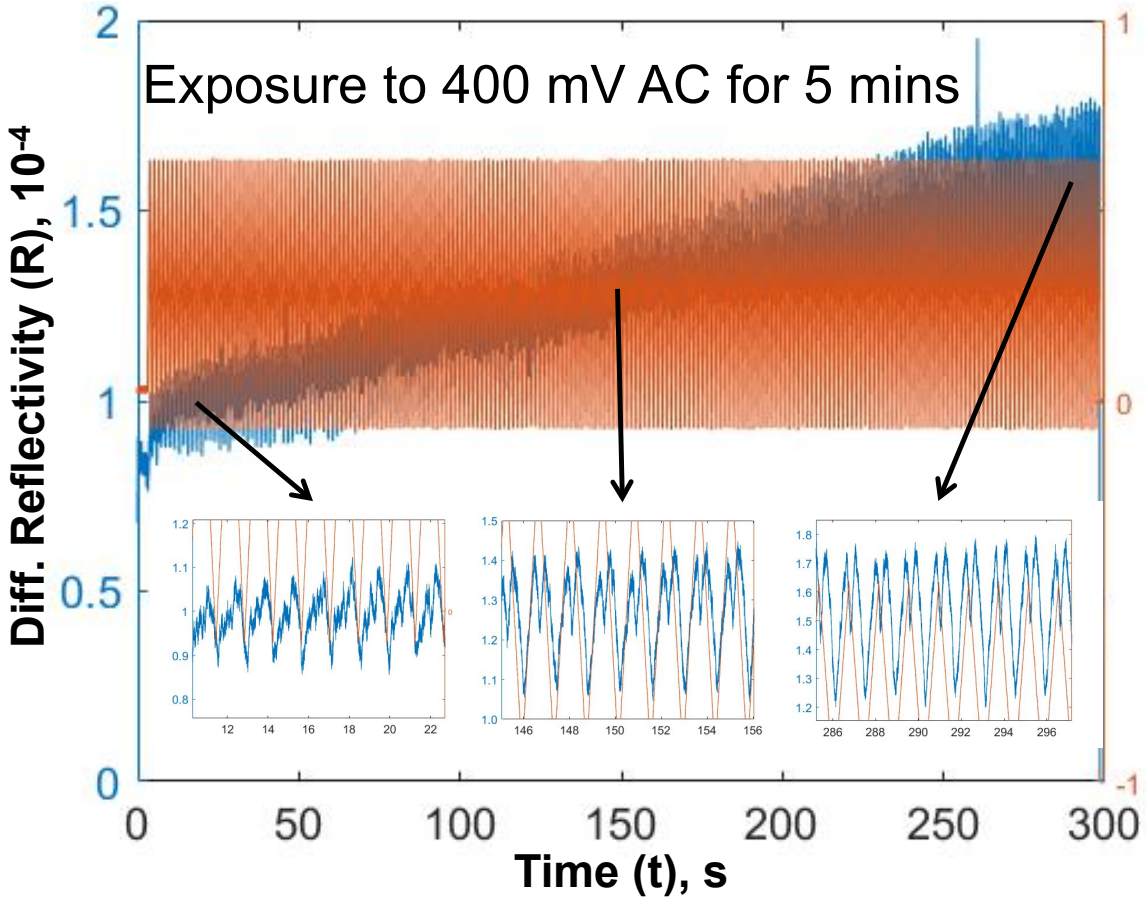

Fig. S8. Real time change in reflectivity at the graphene/Au electrode on exposure to CV cycle with A = 400 mV. The right axis, E(t) (orange) ranges from -0.1 to 0.6 V. The left axis, R(t) (turquoise) is the corresponding response to the applied E(t). The format of the data is similar to raw data in Fig. S3 and S5(a).